Desalination and Water Treatment
www.deswater.com

doi:10.5004/dwt.2018.22578

116 (2018) 317–328
June

Adsorption of Acid Red 114 by facile prepared magnetic amino-nanoadsorbent: Kinetics, isotherms and thermodynamics studies

Mohsen Mohammadi Galangash[a,*], Zahra Niyazi Kolkasaraei[a], Atefeh Ghavidast[a,b], Mehdi Shirzad-Siboni[c,d]

[a]*Department of Environmental Science, Faculty of Natural Resources, University of Guilan, Sowmeh Sara, 1144, Guilan, Iran, Tel./Fax +98 1313233262, email: m_mohammadi@guilan.ac.ir, mohammadi2g@gmail.com (M.M. Galangash), niyazi.z1370@yahoo.com (Z.N. Kolkasaraei), at.ghavidast@yahoo.com (A. Ghavidast)*
[b]*Department of Chemistry, Faculty of Science, University of Guilan, P.O. Box 41335-1914, Rasht, Iran*
[c]*Department of Environmental Health Engineering, School of Health, Guilan University of Medical Sciences, Rasht, Iran, email: mshirzadsiboni@yahoo.com (M. Shirzad-Siboni)*
[d]*Research Center of Health and Environment, Guilan University of Medical Sciences, Rasht, Iran*

Received 1 December 2017; Accepted 5 June 2018

ABSTRACT

Herein, magnetic amino-coated silica iron oxide nanoparticles (Fe_3O_4@SiO_2-NH_2 NPs) were successfully synthesized via a one-pot route and then applied as a nano-adsorbent for removal of Acid Red 114 dye from aqueous solutions. The effect of various experimental parameters such as pH, adsorbent dosage, contact time and initial dye concentration on the dye removal efficiency was studied. According to the experimental results, about 100% of Acid Red 114 was removed from aqueous solutions at the adsorbent amount of 0.4 g L^{-1} at pH = 2 in 120 min. Analysis of kinetics and equilibrium adsorptions revealed that the adsorption data were best fitted to pseudo-second-order kinetic and Langmuir model with the maximum absorption capacity of 84.75 mg g^{-1}, respectively. Furthermore, the Fe_3O_4@SiO_2-NH_2 NPs could be simply recovered by external magnet and it exhibited recyclability and reusability for several cycles. Such functional nanoparticles can be used as effective adsorbents for the removal of organic pollutants from aqueous solutions.

Keywords: Magnetic nanoparticles; Acid Red 114; Amine group; Adsorption; Recycling

1. Introduction

Synthetic dyes have been utilized in many industries including textile, leather, food, cosmetics, electronics, paper, rubber, plastic, printing and pharmaceutical [1–4]. Hence, a large quantity of dye effluents with serious problem to human, micro-organisms and aquatic life are generated from these manufactures [5,6]. Up to now, various techniques such as electrochemical degradation [7–9], ozonation [10], oxidation [11], photocatalysis [12], ion-exchange [13], membrane separation [14,15], adsorption [16–25] and biological process [26,27], have been developed for the treatment of industrial wastewater containing dyes. From these techniques, chemical processes such as oxidation and electrochemical degradation may form harmful and toxic byproducts during the oxidation and degradation of dyes [28]. Among these possible techniques, adsorption has been considered as a more feasible process for most pollutant removal due to low costs, simplicity of design, ease of operation without harmful residues and the possibility of regeneration of the adsorbent [29–31]. Various adsorbents such as activated carbon [32,33], sepiolite [34], vermiculite [35] and magnetic carbon nanotubes [36,37] were successfully used to remove dyes from aqueous solution. Nanostructured materials due to large specific surface area would show potential performance for the adsorption of dyes and toxic

*Corresponding author.

pollutant in wastewater treatment. Although a solid-liquid separation problem restricts their extensive applications. Therefore, the development of magnetic adsorbents is highly desirable. Magnetic nanoparticles (M-NPs) display excellent reusability after many cycles of separation by applying an external magnetic field that is a rapid and economic assessment to remove of target molecules from large volume of toxic waste [38].

Due to low adsorption capacity of NPs, a subsequent surface design and modification is typically required. Until now, various amino-functional groups on the surface of nanomaterials have been reported for the removal of metal ions and synthetic dyes from aqueous solution [39–54]. In the present study, we have successfully synthesized amino-functionalized magnetic Fe_3O_4@SiO_2 NPs (Fe_3O_4@SiO_2-NH_2) via a one-pot direction (Scheme 1) and its efficiency for the removal of Acid Red 114 (AR-114) from aqueous solution is evaluated. The coating of Fe_3O_4 NPs with SiO_2 prevents from agglomeration, oxidation and dissolution of the Fe_3O_4 core in the acidic medium. The Fe_3O_4@SiO_2 NPs was modified with amine groups using 3-aminopropyltriethoxysilane through silanization reaction.

Azo dyes constituting 60–70% of all dyes produced are the largest group of dyes in textile industry and extensively used due to their chemical stability and versatility. They contain one or more azo groups (-N=N-) having aromatic rings mostly substituted by sulfonate groups. Azo dyes are resistant to biodegradation under aerobic conditions [55]. AR-114 is an important azo dye used in textile industry that it has been banned owing to its genotoxic and carcinogenic characteristics and its toxic effects on the nervous systems, blood cells, immune and reproductive systems [56].Although, due to low cost and accessibility, derivatives of these colors may still be used illegally in many developing countries. With the concern of adverse effect of AR-114 on health consequences, potential and efficient methods are needed for the removal of it from water.

The adsorption performance of the Fe_3O_4@SiO_2-NH_2 NPs for AR-114 from aqueous solution has been systematically investigated by the effect of various parameters including pH, contact time, the adsorbent amount and dye concentration. In addition, the adsorption isotherm, kinetics, thermodynamics feature and the reusability of the adsorbents are also analyzed.

2. Experimental

2.1. Materials and apparatus

The following reagents were purchased from Merck and used without further modification: ferric chloride hexahydrate ($FeCl_3{\cdot}6H_2O$), ferrous chloride tetrahydrate ($FeCl_2{\cdot}4H_2O$), ammonium hydroxide (NH_4OH, 25 wt %), tetraethylorthosilicate (TEOS) and 3-aminopropyltriethoxysilane(APTES). AR-114 was purchased from Sigma-Aldrich (purity = 80%). A pH meter (Metrohm, model 713, Swiss) was used for pH measurements. The UV-Vis absorption spectra in the range of 200–700 nm were measured with a Shimadzu UV-2100 spectrophotometer. Spectral data were obtained using quartz cuvettes with 1 cm optical path length. The FT-IR spectra for the samples were obtained using Shimadzu FT-IR-8900 spectrometer by using KBr pellets. The X-ray diffraction (XRD) patterns were recorded in air at ambient temperature by Phillips (pw-1840) X-ray diffractometer with Cu-Kα radiation source (λ = 1.54056 Å) at 40 kV voltage and 25 mA current in a wide angle range (2θ = 20–70°). The TEM samples were prepared by suspending the NPs in EtOH followed by sonication for several minutes. One drop of the dilute NPs/EtOH suspension was placed on a carbon-coated holey TEM copper grid and was dried in air. The dried grid was then loaded into a double tilt sample holder. The sample was then examined with a Philips CM-20 STEM equipped with a GatanUltraScan 1000 CCD camera and an energy dispersive X-ray spectrometer: INCA Energy TEM 200. TEM images were taken at 200 KV.

2.2. One-pot synthesis of Fe_3O_4@SiO_2-NH_2 NPs

Fe_3O_4@SiO_2-NH_2 NPs were synthesized in the following continuous one-pot process without powder drying and as consecutive (Fig. 1): At first, 1.0 g of $FeCl_3{\cdot}6H_2O$ and 0.36 g of $FeCl_2{\cdot}4H_2O$ were dissolved in 20 ml of deionized H_2O. Then, 1 ml of NH_3 was added drop-wise to the solution via a dropping funnel under vigorous stirring. The reaction was refluxed at 80°C for 5 h under an N_2 atmosphere. The obtained Fe_3O_4 precipitant was separated with a magnet and was repeatedly washed with deionized H_2O and re-dispersed in 50 mL of H_2O.Then, 1 ml TEOS in 20 mL EtOH, was added to solution, followed by rapid inversion mixing at 80°C for 24 h under N_2 atmosphere. The obtained black powder Fe_3O_4@SiO_2 was separated with magnet and was washed with H_2O and EtOH tree times. Subsequently, this achieved NPs without drying suspended in 10 mL of EtOH and stirred heavily for 15 min under N_2 gas. Then, 0.37 mL of APTES in 25 mL of EtOH was added drop-wise to resulting mixture under mechanical stirring. The reaction was refluxed at 80°C for 8 h at N_2 atmosphere. The resulted mixture was cooled and the solid was separated magnetically and then washed with EtOH and H_2O several times (3 × 50 mL).The precipitate was then dried in oven at 50°C for 8 h and the black nanopowder Fe_3O_4@SiO_2-NH_2 was obtained.

2.3. Adsorption studies

The adsorptive removal of AR-114 was carried by batch experiments. Tests were conducted in 500 mL conical flasks containing 20 mg L^{-1}AR-114 solution in a water bath to elucidate the values of the test parameters including solution pH (2–11), dye concentration (10–100 mg L^{-1}), temperature (298 K) and absorbent dosage (0.1–0.5 g L^{-1}). The pH of the solution was adjusted by dropwise addition of 0.1 M HCl or 0.1 M NaOH. After each removal condition experiments, the samples were separated from the dye solution with a permanent magnet and the residual dye molecules concentrations in the solution were determined by UV-Vis spectrophotometer at 515 nm for AR-114. Also, the zero point charge (pH_{zpc}) of Fe_3O_4@SiO_2-NH_2 was determined. Adsorbent (0.2 g) was added to 40 mL of 0.1 M $NaNO_3$ solutions at various initial pH in the range of 2–11. The initial pH of solutions was adjusted by the addition of 0.1 M NaOH or

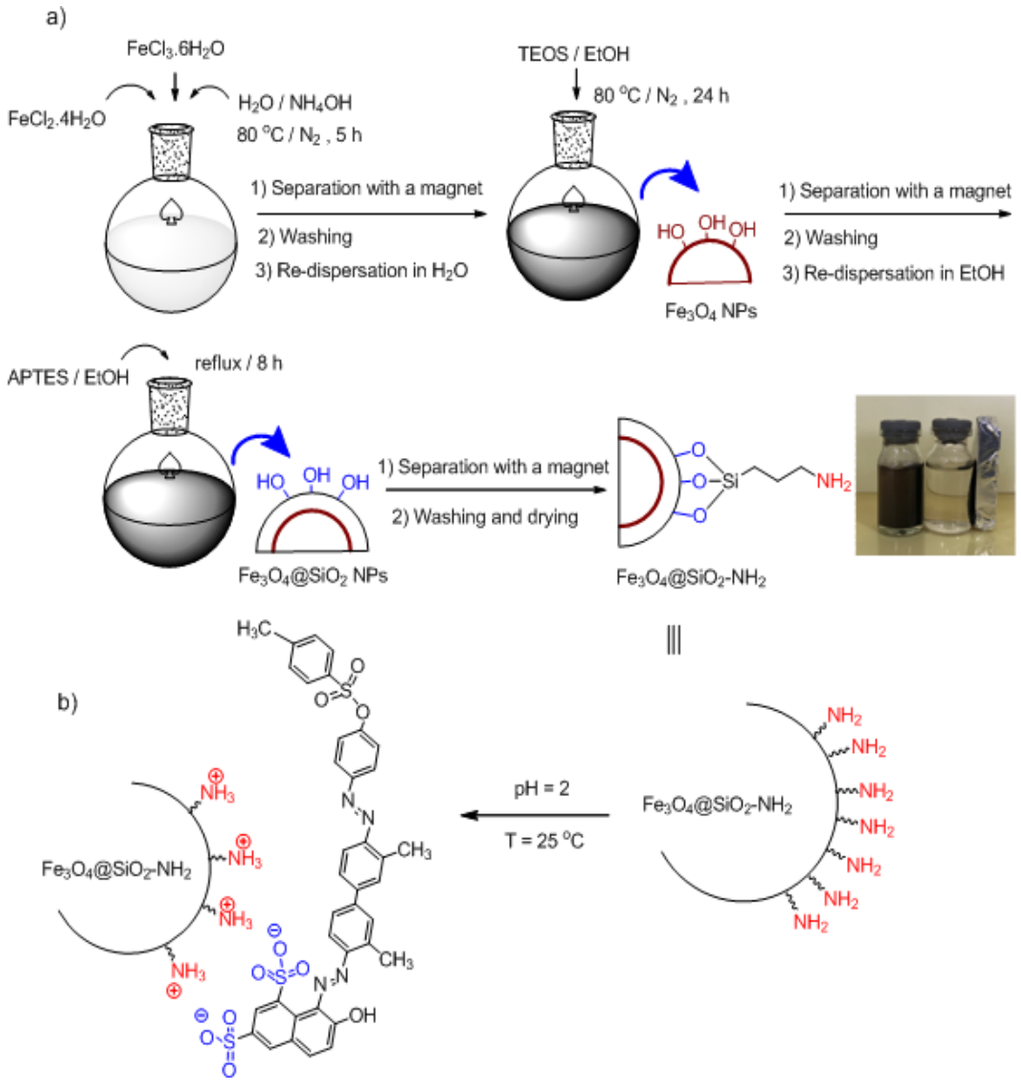

Fig. 1. (a) One-pot synthesis of Fe_3O_4@SiO_2-NH_2NPs and (b) its interactions with AR-114.

HCl, and measured by pH meter. Afterward, the mixtures were shaken on a rotary shaker (KS-15, Edmund Buhler, Germany) at 170 rpm for 48 h at room temperature, and the final pH of each solution was measured at equilibrium.

2.4. Desorption and reusability experiments

Desorption was investigated separately for 20 mg L^{-1} AR-114 in 500 mL. The sorbent was rinsed with 20 mL of 0.01 M NaOH that was sufficient for complete desorption of the dye. In order to increase the recoveries; 10 min vortex was used after each washing step. The UV-Vis test of the upper layer solution after vortex was applied to make sure all the AR-114 was recovered. The concentration of each eluent was measured using the obtained standard curve from spectrophotometry method. For reusability test, the sorbent was washed 5 times with 20 mL of 0.01 M NaOH aqueous solutions (each step with 4 mL solvent and 10 min vortex) after dye extraction. Then, the sorbent was rinsed with H_2O to remove the NaOH excess and dried at 40°C in an oven.

3. Results and discussion

In continuation to our prior works [57–60] herein, the modified magnetic Fe_3O_4@SiO_2-NH_2NPs were synthesized by the one-pot procedure as shown in Fig. 1. Firstly, Fe_3O_4 NPs were prepared by co-precipitation of Fe^{2+} and Fe^{3+} ions in basic solution and then in order to avoid possible aggregation or oxidation of the Fe_3O_4 NPs surfaces, a layer of SiO_2 using sol-gel process, through the hydrolysis of TEOS was coated on Fe_3O_4 NPs surfaces and successfully, Fe_3O_4@SiO_2 core-shell microspheres were prepared. Subsequently, Fe_3O_4@SiO_2 core-shell was reacted with APTES as a spacer to obtain amino-functionalized Fe_3O_4@SiO_2-$NH_2$and the success of this immobilization was monitored with FT-IR, XRD and TEM.

3.1. Fourier transform infrared spectroscopy

The FT-IR spectrum of prepared Fe_3O_4@SiO_2-NH_2(red line) that compared with Fe_3O_4 NPs (black line) and Fe_3O_4@SiO_2 NPs (violet line) is shown in Fig. 2. The typical absorption peaks at 567 cm^{-1} is related to the stretching vibration of Fe-O bond and overlap with stretching bonds of Si-O-Fe. The characteristic absorption bands at 1000, 3417 and 2869–2906 cm^{-1} are corresponded to C-N, N-H and C-H stretching modes of the alkyl chain, respectively and the N-H bending mode appeared at 1627 cm^{-1} that confirm the successful coating of APTES on Fe_3O_4@SiO_2 surfaces [58].

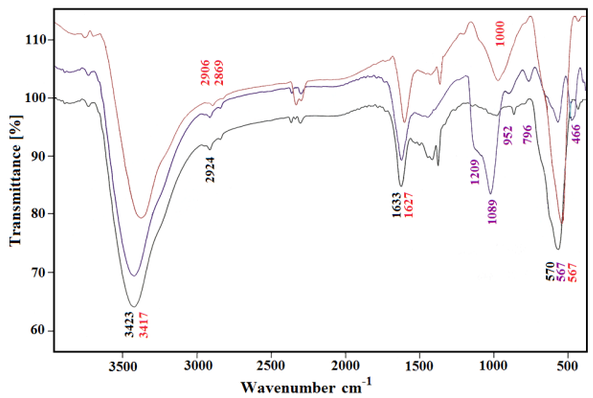

Fig. 2. The FT-IR spectra of Fe_3O_4@SiO_2-NH_2 (red line), Fe_3O_4@SiO_2 NPs (violet line) and Fe_3O_4 NPs (black line).

3.2. Transmission electron microscopy image and X-ray diffraction

Fig. 3 shows the transmission electron microscopy (TEM) images of Fe_3O_4@SiO_2-NH_2 NPs (Fig. 3a), Fe_3O_4@SiO_2 NPs (Fig. 3b), Fe_3O_4 NPs (Fig. 3c) and the X-ray diffraction (XRD) patterns of Fe_3O_4@SiO_2-NH_2 (Fig. 3d). The Fig. 3a, confirms that the functional group (with light color) is immobilized on the surface of Fe_3O_4@SiO_2 NPs (with dark color), obviously. The synthesized Fe_3O_4@SiO_2-NH_2 NPs showed a spherical shape with an average diameter of about <20 nm, however, the NPs tended to aggregate to large particle. The pure Fe_3O_4@SiO_2 NPs (Fig. 3b) and Fe_3O_4 NPs (Fig. 3c) appear to be almost spherical in shape with a diameter range about < 15 and 10 nm, respectively. TEM analysis reveals that the presence of SiO_2 and APTES shell increase the size of magnetite NPs [58].

In the Fig. 3d, sharp diffraction peaks with 2θ at 30.3° (220), 35.6° (311), 43.3° (400), 53.9°(422), 57.2° (511) and 62.5° (440) are observed, which indicate that the Fe_3O_4@SiO_2-NH_2 particles have highly crystalline cubic spinel structure of the magnetite. The average crystallite size D was determined by the Scherrer formula, $D = K\lambda/(\beta\cos\theta)$, where λ = 1.54 Å is the wavelength of Cu-Kα radiation used, β is the full width at half-maximum (FWHM) intensity of the diffraction line, θ is the Bragg angle for the measured *hkl* peak (Miller indices) and K is a constant equal to 0.94. The particle sizes of the magnetite calculated using the Scherrer equation was 15.7 nm [61]. This value is in good agreement with that obtained from TEM image.

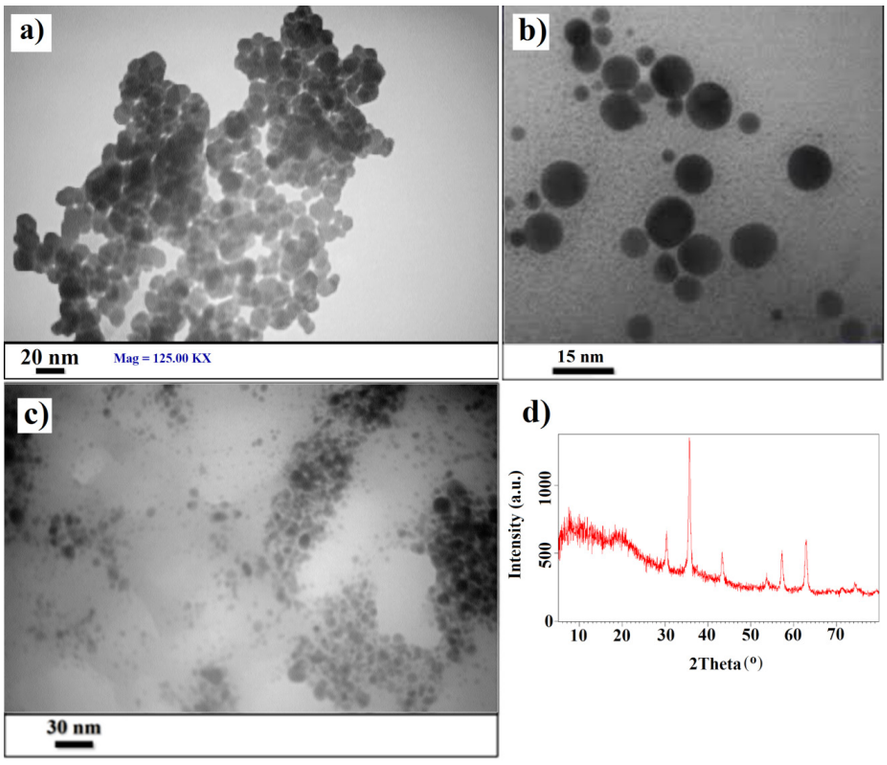

Fig. 3. TEM micrographs of (a) Fe_3O_4@SiO_2-NH_2 NPs, (b) Fe_3O_4@SiO_2 NPs, (c) Fe_3O_4 NPs and (d) XRD pattern of Fe_3O_4@SiO_2-NH_2 NPs.

3.3. Effect of pH on adsorption

The pH of the aqueous solution is the very crucial parameter for its effect on the surface charge of the adsorbents, the degree of ionization and speciation of the adsorbates [62]. The effect of initial pH on the AR-114adsorption by Fe_3O_4@SiO_2-NH_2surfaces at different values, ranging 2–11 and with a constant time 180 min is shown in Fig. 4. The initial concentration of dye and adsorbent dosage were kept fixed at 20 mg L^{-1} and 0.3 g L^{-1}, respectively. As was expected, the results demonstrated that the uptake amount strongly depends on solution pH. Maximum removal efficiency of AR-114 onto Fe_3O_4@SiO_2-$NH_2$was observed at the initial pH = 2 (98.69%), and reduced dramatically when solution pH increased and turned to alkali, which could be due to the ionization of amine groups of adsorbent at pH above the pK_a. The pK_a value of alkyl amines is approximately 10.6 at 298 K and amine groups of Fe_3O_4@SiO_2-NH_2 existed as protonated form in the range of pH < pK_a. Therefore, change to ammonium cation at pH < pK_a with hydrophilic nature and a strong electrostatic interaction occurred between the positively charged amine groups on the adsorbent surface and negative AR-114 molecules (Fig. 1) [63]. In addition, in basic pH, the OH^- ions compete with dye anions for the adsorption sites of Fe_3O_4@SiO_2-NH_2. Adsorption studies were applied to pH = 11 even though adsorption is high at acidic medium due to stability of AR-114 dye in wide range of pH. It is known that acid dyes, on dissolution, release colored dye anions in to solution. The adsorption of these anionic charged groups onto the adsorbent surface is mainly influenced by the surface functional groups on the adsorbent, which in turn is influenced by the solution pH [58].

In order to obtain further information about the surface charge of the adsorbent, the point of zero charge (pH_{ZPC}) was also determined. The difference between $pH_{initial}$ and pH_{final} is illustrated in Fig. 5, which shown the point of zero charge is around 8.0. This means that at pH values below 8, the Fe_3O_4@SiO_2-NH_2 NPs surface has a net positive charge and the electrostatic attraction force exists between adsorbent and AR-114 as a polar molecule (R-SO_3^-), while at pH greater than 8, the surface has a net negative charge and the electrostatic repulsion force exists between adsorbent and adsorbate. Hence, the acidic pH facilitates the adsorption of AR-114 onto Fe_3O_4@SiO_2-NH_2 surface and maximum removal percentage and adsorption capacity take place at pH = 2.

3.4. Effect of adsorbent dose on adsorption

The adsorption of dye on Fe_3O_4@SiO_2-NH_2NPs was investigated by changing the quantity of adsorbent range of 0.1–0.5 g L^{-1}, with the dye concentration of 20 mg L^{-1}, room temperature (25 ± 1°C) and pH = 2 for different time intervals (0–180 min). The results in Fig. 6 show that with the increase in adsorbent dosage from 0.1 to 0.5 g L^{-1}, the percentage adsorption increases from 67.39 to 100% over the entire contact time 180 min due to the increased surface area and further active binding sites [64]. Furthermore, the rate of removal of AR-114 at adsorbent dosages of 0.4 and 0.5 g L^{-1} is primarily rapid in the first stage of contact time and then it is gradually slowed until reactions reach equilibrium that attributed to the large quantity of free active sites on

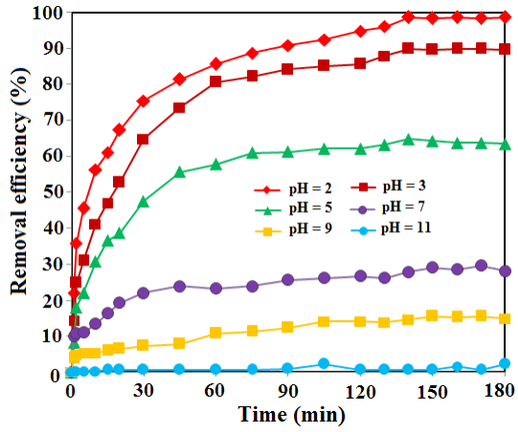

Fig. 4. The effect of pH on the adsorption of AR-114 on Fe_3O_4@SiO_2-NH_2 in different time interval ([AR-114]$_0$ = 20 mg L^{-1} and adsorbent dosage = 0.3 g L^{-1}).

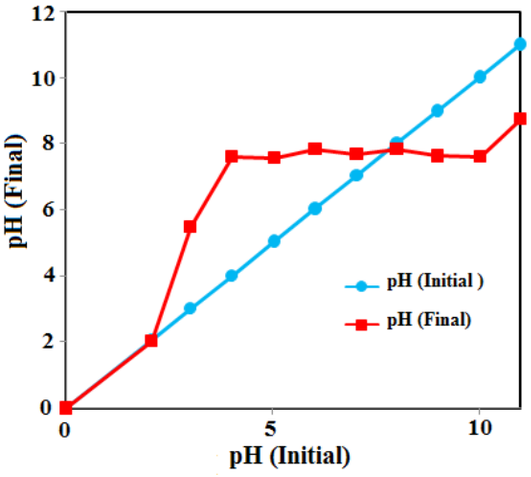

Fig. 5. Determination of the pH of point of zero charge (pH_{ZPC}).

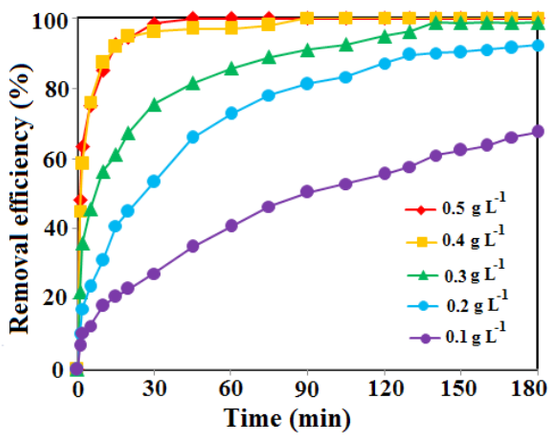

Fig. 6. The effect of adsorbent dose on the adsorption of AR-114 on Fe_3O_4@SiO_2-NH_2 in different time interval ([AR-114]$_0$ = 20 mg L^{-1} and pH = 2).

the Fe_3O_4@SiO_2-NH_2 surface and convenient accessibility of them for AR-114 molecules [65]. Since the removal efficiency of AR-114 does not significant difference between dosage 0.4 and 0.5 g L^{-1}, further bath adsorption experiments were carried out at 0.4 g L^{-1}. In fact, the removal efficiency enhanced from 45.07 to 100% by increasing the contact time from 0.5 to 90 min at pH = 2 and adsorbent dosage equal to 0.4 g L^{-1}.

3.5. Effect of contact time on adsorption

To know the equilibration time for maximum adsorption, the adsorption of AR-114 on the Fe_3O_4@SiO_2-NH_2NPs surface was studied at different contact time of 1–180 min (Fig. 7). It was observed that the adsorption of AR-114 increased fast in the first and almost 90% adsorption was completed within 10 min, and then slowed down until the sorption process reaches equilibrium after 120 min. Therefore 120 min was selected as optimum time and equilibrium time for adsorption process of AR-114 on the Fe_3O_4@SiO_2-NH_2 surface at the concentration of AR-114 20 mg L^{-1}, pH = 2, temperature 298 K and adsorbent dosage 0.4 g L^{-1}. The dye adsorption processes are shown in the inset of Fig. 7.

3.6. Effect of initial dye concentration on adsorption

The adsorbate initial concentration acts as an important driving force to overcome the mass transfer resistance of dye between the aqueous and the solid phases [66]. The effects of initial dye concentrations on the rate of adsorption by Fe_3O_4@SiO_2-NH_2NPs were studied in four solutions of different initial AR-114 concentrations 10, 20, 40, 60, 80 and 100 mg L^{-1} (Fig. 8). Fig. 8 shows that by increasing the initial dye concentration from 10 to 100 mg L^{-1}, the percentages of dye removal decreased from 100.00 to 46.38. In fact, by increasing the initial dye concentration, the number of vacant binding sites and adsorption driving forces in solutions decreased [67].

3.7. Adsorption kinetics

Adsorption kinetic experiments were analyzed at different AR-114 concentration = 10, 20, 40, 60, 80 and 100 mg L^{-1}, constant adsorbent dosage = 0.4 g L^{-1} and pH = 2. The pseudo-first-order, pseudo-second-order and intra-particle-diffusion models were applied in order to find an efficient model for the description of adsorption mechanism. The pseudo-first-order kinetic model is expressed as follow [68]:

$$\ln(q_e - q_t) = \ln(q_e) - k_1 t \quad (1)$$

where q_e and q_t are the amount of dye adsorbed at equilibrium (mg g^{-1}) and amount of dye adsorbed at time t (mg g^{-1}), respectively; k_1 (min^{-1}) is the rate constant of the pseudo-first-order adsorption. Using this equation, the values of k_1 and q_e were calculated from the slope and intercept of the plot of $\ln(q_e - q_t)$ versus t, respectively [69].

The pseudo-second-order kinetic model can be expressed as follow:

$$\frac{t}{q_t} = \frac{1}{k_2 q_e^2} + \left(\frac{1}{q_e}\right) t \quad (2)$$

where k_2 is the rate constant of pseudo-second-order adsorption (g mg^{-1} min^{-1}). The slope and intercept of the plot of t/qt versus t were used to calculate the pseudo-second-order rate constant.

The possibility of intra-particle diffusion resistance affecting adsorption was investigated using the intra-particle diffusion model as [70]:

$$q_t = k_p t^{1/2} + C \quad (3)$$

where k_p (mg g^{-1} $min^{-1/2}$) is the intra-particle diffusion rate constant which can be evaluated from the slope of the linear plot of q_t versus $t^{1/2}$, and C (mg g^{-1}) is intercept. Values of C give an idea about the thickness of the boundary layer: the larger the intercept, the greater the boundary layer effect.

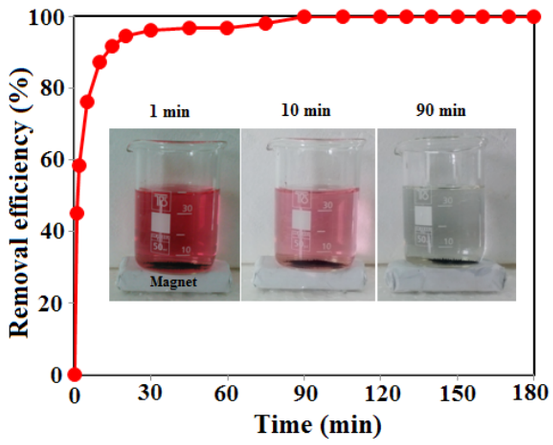

Fig. 7. The effect of contact time on the adsorption of AR-114 on Fe_3O_4@SiO_2-NH_2 in different contact time interval. The inset figures show photographs of aqueous solutions of AR-114 before and after adsorption (1–90 min vortex). ($[AR\text{-}114]_0$ = 20 mg L^{-1}, adsorbent dosage = 0.4 g L^{-1} and pH = 2).

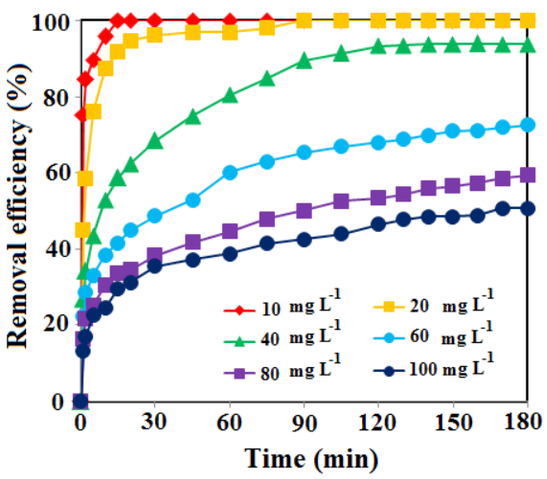

Fig. 8. The effect of initial dye concentrations on the adsorption of AR-114 on Fe_3O_4@SiO_2-NH_2 in different contact time interval (adsorbent dosage = 0.4 g L^{-1} and pH = 2).

The best-fit model was selected based on the linear regression correlation coefficient R^2 values. The kinetic parameters for the removal AR-114 at different initial concentrations by three models are summarized in Table 1. The results show that first-order kinetic and intra-particle diffusion models are not suitable for the present adsorption system due to low correlation coefficients R^2. Moreover, a large difference between $q_{e.exp}$ and $q_{e.cal}$ was observed, indicating a poor pseudo-first-order fit to the experimental data. The kinetic data for AR-114 adsorption showed the best fitting (R^2 = 0.9999) with the pseudo-second-order model and the calculated q_e values also agree very well with the experimental data (Fig. 9). Similar results were reported for the adsorption kinetics of various pollutants onto activated carbon cloth [71,72]. Moreover, when the initial AR-114 concentration increased from 10 to 100 mg L^{-1}, the value of k_2 (g mg^{-1} min^{-1}) and R^2 for the pseudo-second-order model were decreased from 0.0558 to 0.00056 g mg^{-1} min^{-1} and 0.9996 to 0.9907, respectively. Also, $q_{e,cal}$ (mg g^{-1}) increased from 27.62 to 126.58 mg g^{-1}. This result indicated that adsorption data were in agreement with this model. Based on the kinetic model obtained, a chemisorption bond takes place during adsorption of AR-114 on the Fe_3O_4@SiO_2-NH_2 NPs surface. For the intra-particle diffusion model the value of C was calculated as 36.298 mg g^{-1} ($C \neq 0$), indicates that intra-particle diffusion was not the only rate-limiting step for AR-114 adsorption and the adsorption procedure involves more than one diffusive resistance.

3.8. Adsorption isotherm studies

The evaluation of adsorption isotherms is important for developing a model for adsorbent-adsorbate interactions [73,74]. The adsorption isotherms of AR-114 on the Fe_3O_4@SiO_2-NH_2NPs with 20 mg L^{-1} AR-114 as an initial concentration using various adsorbent dosages (0.05–1 g L^{-1}) at pH = 2 for 72 h at different temperatures are given in Fig. 10, and the equilibrium adsorption data were evaluated according to the renowned models Langmuir and Freundlich isotherms.

The Langmuir isotherm supposes that monolayer adsorption takes place at binding sites with homogenous energy levels, without interactions between adsorbed molecules and transmigration of adsorbed molecules onto adsorption surface. The Langmuir equations can be expressed as [75]:

$$q_e = \frac{q_m k_l C_e}{1 + k_l C_e} \tag{4}$$

or

$$\frac{C_e}{q_e} = \frac{1}{k_l q_m} + \frac{1}{q_m} C_e \tag{5}$$

where C_e is the equilibrium concentration of the AR-114 solution (mg L^{-1}), q_e is the adsorption capacity at equilibrium (mg g^{-1}), k_l is the constant related to free energy of adsorption (L mg^{-1}), and q_m is the maximum adsorption capacity at monolayer coverage (mg g^{-1}).

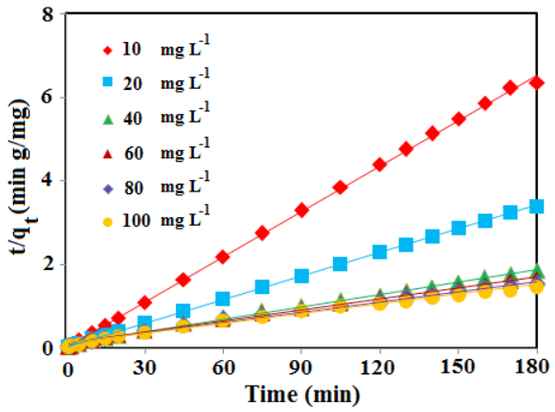

Fig. 9. The linear plots of pseudo-second-order model of the AR-114 removal by Fe_3O_4@SiO_2-NH_2 in different time and concentration (pH = 2 and adsorbent dosage = 0.4 g L^{-1}).

Table 1
Kinetic parameters for AR-114 adsorption onto Fe_3O_4@SiO_2-NH_2

Kinetic models	$[AR\text{-}114]_0$ (mg L^{-1})					
	10	20	40	60	80	100
$q_{e,exp}$ (mg g^{-1})	28.30	53.30	96.63	107.08	117.44	122.86
Pseudo-first-order						
k_1 (min^{-1})	0.0067	0.0157	0.0265	0.0222	0.0197	0.0235
$q_{e,cal}$ (mg g^{-1})	12.04	5.95	1.59	1.34	1.32	2.23
R^2	0.3632	0.765	0.9726	0.9781	0.934	0.8022
Pseudo-second-order						
k_2 (g mg^{-1} min^{-1})	0.0558	0.0106	0.0011	0.00066	0.00059	0.00056
$q_{e,cal}$(mg g^{-1})	27.62	53.19	101.01	112.36	120.48	126.58
R^2	0.9996	0.9999	0.9975	0.9941	0.9899	0.9907
Intra-particle diffusion						
K_p (mg g^{-1} $min^{-1/2}$)	0.3646	1.4803	5.3213	6.2609	6.5534	7.137
C_0 (mg g^{-1})	23.55	36.298	33.974	29.907	33.243	32.707
R^2	0.4936	0.6044	0.9267	0.9646	0.9788	0.9599

The Freundlich isotherm is a practical equation that supposes heterogeneous adsorbent surface with its adsorption sites at changeable energy levels [76]. The corresponding equations are common lyre presented by:

$$q_e = k_f C_e^{1/n} \tag{6}$$

or

$$\ln q_e = \ln k_f + \frac{1}{n}\ln C_e \tag{7}$$

k_f (mg$^{1-(1/n)}$ L$^{1/n}$ g^{-1}) and n are the Freundlich constants characteristics of the system, indicating the adsorption capacity and the adsorption intensity, respectively. If the value of $1/n$ is lower than 1, it indicates a normal Freundlich isotherm; if not, it is indicative of cooperative adsorption [77].

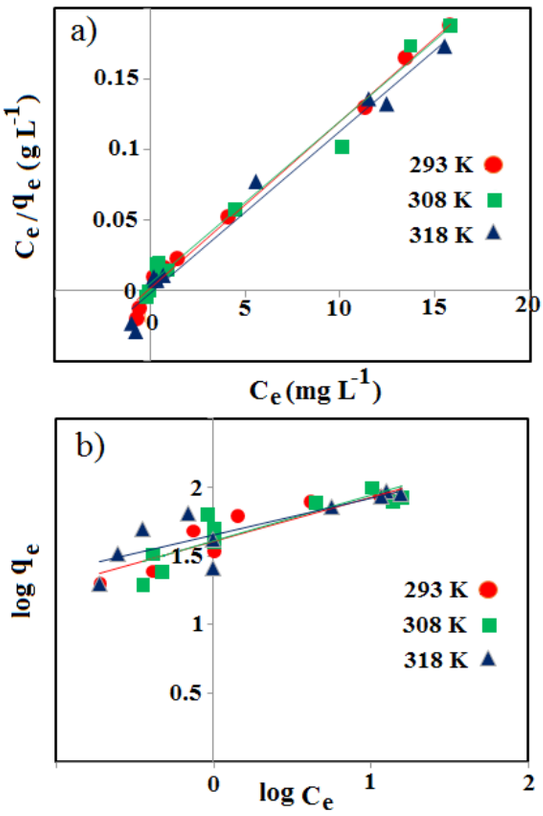

Fig.10. The plots of (a) Langmuir isotherm and (b) Freundlich isotherm for the AR-114 adsorption onto the Fe_3O_4@SiO_2-NH_2 at different temperatures (pH = 2, $[AR\text{-}114]_0$ = 20 mg L^{-1}, adsorbent dosage = 0.05–1 g L^{-1} and time = 72 h).

The calculated isotherm parameters from both models are shown in Table 2. The adsorption of AR-114 was fit to the Langmuir isotherm model better than Freundlich with the higher R^2 (0.9906). It indicates that the adsorption occurred at specific homogeneous sites with in the adsorbent forming monolayer coating of AR-114 at the surface of the adsorbent. The Freundlich constant $1/n$ was smaller than 1, indicating a high adsorption intensity (Table 2). Table 2 also shows that the maximum monolayer adsorption capacity of (q_m) AR-114 by Fe_3O_4@SiO_2-NH_2NPs was 84.75 mg g^{-1} in 293 K and increased above it. This may be attributed to increased surface coverage at higher temperature, expansion and creation of reactive and active sites.

The adsorption isotherm process favorability was also evaluated using the dimensionless separation factor (R_L) that were calculated using the following equation [78]:

$$R_L = \frac{1}{1 + k_1 C_0} \tag{8}$$

The adsorption process can be defined as favorable ($0 < R_L < 1$), unfavorable ($1 < R_L$), linear ($R_L = 1$) and irreversible in nature ($R_L = 0$) [79]. In this study, the value of R_L calculated for the adsorption of AR-114 by Fe_3O_4@SiO_2-NH_2 fall between 0 and 1 (R_L = 0.008), therefore, theadsorptionofAR-114 onto the adsorbent appears to be a favorable process.

3.9. Desorption and recycling studies

Several (adsorption-desorption) regeneration cycles with Fe_3O_4@SiO_2-NH_2 NPs were performed by 20 mL 0.01 M NaOH solution, as shown in Fig. 11. In fact, the AR-114 molecules on the surface of Fe_3O_4@SiO_2-NH_2 NPs could be replaced with hydroxyl ions of the basic solution in adsorbent washing step. The result showed the recovery values were not significantly decreased and reused for at least four successive removal processes with removal efficiency higher than 88% that display the stability of adsorbent. Fig. 11c shows the TEM image of the Fe_3O_4@SiO_2-NH_2NPs after the fourth cycle of adsorption/desorption. The result indicates that Fe_3O_4@SiO_2-NH_2NPs were not significantly altered during the regeneration process. Also, after five cycles of the desorption-adsorption process, the high magnetic sensitivity of Fe_3O_4@SiO_2-NH_2NPs still retained and was collected from the solution using a magnet of 1.4T (right inset in Fig. 11). Therefore, the Fe_3O_4@SiO_2-NH_2NPs can be potentially used as a magnetic adsorbent for further dye adsorption from water.

Table 2
Adsorption isotherm parameters for AR-114 adsorption on the Fe_3O_4@SiO_2-NH_2 NPs

T (K)	Langmuir isotherm				Freundlich isotherm		
	q_m (mg g^{-1})	k_1 (L mg^{-1})	R^2	R_L	k_f (mg$^{1-(1/n)}$ L$^{1/n}$ g^{-1})	n	R^2
293	84.7458	6.2112	0.9906	0.008	40.2346	3.0921	0.8605
308	86.9565	2.2114	0.9839	0.0221	40.7193	3.0423	0.7835
318	86.9565	8.8496	0.9800	0.0056	44.5143	3.7161	0.7044

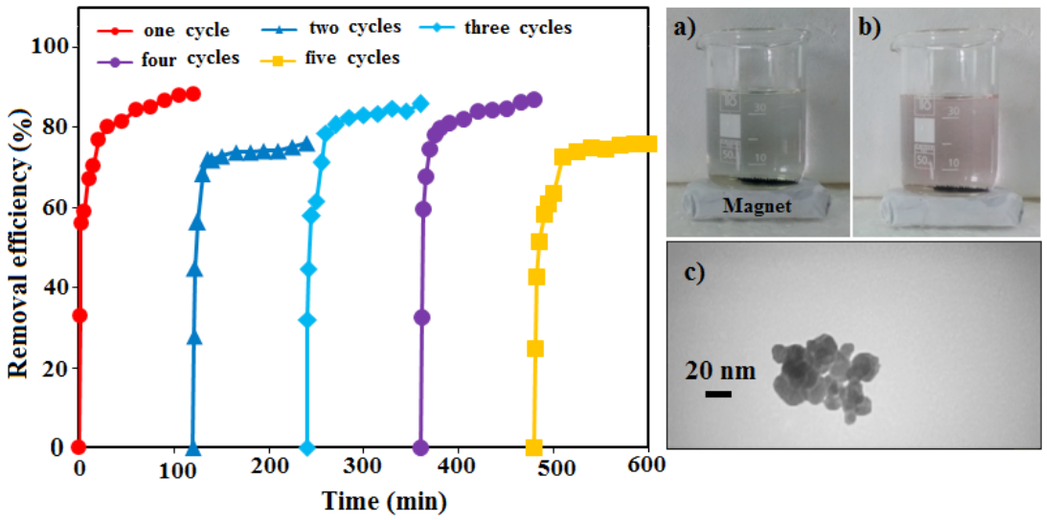

Fig. 11. The removal efficiency during five cycles of Fe_3O_4@SiO_2-NH_2. The inset figures show aqueous solutions of AR-114 (a) after one cycle adsorption, (b) after five cycles of desorption-adsorption and (c) the TEM image of the Fe_3O_4@SiO_2-NH_2 after the fourth cycle adsorption/desorption.

Table 3
Comparison of various adsorbents for AR-114 removal

Adsorbents	pH	Temperature (K)	q_m (mg g^{-1})	Best fit isotherm	Ref.
Activated carbon	–	293	103.73	Both	[80]
AAEC[a]	1.5	303	112.34	Langmuir	[81]
KTC[b]	7.02	300	450.02	Freundlich	[82]
CPAC[c]	6	303	69.45	Langmuir	[83]
ICAC[d]	6	303	80.86	Langmuir	[84]
Activated carbon-Pp[e]	3	298	204.08	Langmuir & Freundlich	[85]
Activated carbon-Cp[f]	3	298	153.85	Langmuir & Freundlich	[85]
Activated carbon-Sp[g]	3	298	102.04	Langmuir & Freundlich	[85]
SBA-3/PEHA[h]	6	293	1000	Freundlich	[86]
Fe_3O_4	6	293	111	Freundlich	[87]
Fe_3O_4@SiO_2-MPAP[i]	2	298	105.26	Langmuir	[58]
Fe_3O_4@SiO_2-NH_2	2	298	84.75	Langmuir	This work

[a]Acid-activated eichorniacrassipes (an activated plant biomass)
[b]Kattamanakku tree leaf powder carbon
[c]Ceiba Pentradenta wood waste- activated carbon@H_3PO_4
[d]Ipomeacarnea stem waste@phosphoric acid
[e]Activated pongam seed shells
[f]Activated cotton seed shells
[g]Activated sesame seed shells
[h]Pentaethylene hexamine functionalized SBA-3
[i]Methyl propylaminopropanoate-coated Fe_3O_4@SiO_2 nanoparticles

3.10. A comparison with other adsorbents

A comparison between results of the performance of Fe_3O_4@SiO_2-NH_2 with other adsorbents on removal of dyes in the previous studies is presented in Table 3 [58,80–87]. Table 3 clearly presents that several efficient adsorbents have already been synthesized; however the absorption capacity of Fe_3O_4@SiO_2-NH_2 NPs could be comparable or even better than the natural inorganic and agricultural by-products adsorbents. In the Fe_3O_4@SiO_2-NH_2 NPs compared to Fe_3O_4 NPs (entry 10), a thin and dense SiO_2 layer along with a desired thickness of APTES shell can protect the iron oxide core from leaching out under acidic conditions [87]. Hence, the stability of Fe_3O_4@SiO_2-NH_2 NPs increases. It is noticeable that the higher adsorption capacity of SBA-3/PEHA (entry 9) is due to electrostatic interaction and hydrogen bond formation between the surface

of the adsorbent and AR-114, simultaneously [85]. Additionally, the adsorption capacity of Fe_3O_4@SiO_2-NH_2 as a result of electrostatic interaction is lower than Fe_3O_4@SiO_2-MPAP [58]. These results demonstrate that the hydrogen bond formation plays more important function in AR-114 adsorption than electrostatic interaction. Furthermore, the magnetic properties of Fe_3O_4@SiO_2-NH_2 make it more efficient adsorbent for the removal of contaminant from aqueous solution.

4. Conclusion

Here, magnetic amino-modified adsorbent Fe_3O_4@SiO_2-NH_2 NPs have been successfully prepared through a facile and one-pot process and used for the removal of AR-114 from aqueous solution. The decolorization efficiency depended on experimental parameters including contact time, initial dye concentration, the amount of adsorbent and pH. The removal efficiency at optimum pH = 2 was found to increase with increase in contact time and adsorption dosage, but to decrease with increase in initial dye concentration. Analysis of the Fe_3O_4@SiO_2-NH_2 NPs by XRD, FT-IR and TEM revealed crystal structure, functional groups and a spherical shape with an average diameter of about < 20 nm contributed in the dye adsorption. The adsorption kinetics and isotherms were examined in detail. The adsorption followed pseudo-second-order kinetics. The equilibrium data fitted well the Langmuir isotherm with the maximum absorption capacity of 84.75 mg g^{-1}. The experimental results showed that the Fe_3O_4@SiO_2-NH_2 NPs could be utilized as a promising and efficient adsorbent for the environmental cleanup.

Acknowledgments

This study was supported in part by the Research Committee of University of Guilan& Iran Nanotechnology Initiative Council (INIC).

References

[1] L. Ai, L. Lili, Efficient removal of organic dyes from aqueous solution with ecofriendly biomass-derived carbon@montmorillonite nanocomposites by one-step hydrothermal process, Chem. Eng. J., 223 (2013) 688–695.
[2] X. Li, C. Zeng, J. Jiang, L. Ai, Magnetic cobalt nanoparticles embedded in hierarchically porous nitrogen-doped carbon frameworks for highly efficient and well-recyclable catalysis, J. Mater. Chem. A, 4 (2016) 7476–7482.
[3] Q. Liu, C. Zeng, L. Ai, Z. Hao, J. Jiang, Boosting visible light photoreactivity of photoactive metal-organic framework: Designed plasmonic Z-scheme Ag/AgCl@MIL-53-Fe, Appl. Catal. B., 224 (2018) 38–45.
[4] M. Akgül, Enhancement of the anionic dye adsorption capacity of clinoptilolite by Fe^{3+}-grafting, J. Hazard. Mater., 267 (2014) 1–8.
[5] C.X. Wang, A. Yediler, D. Lienert, Z.J. Wang, A. Kettrup, Toxicity evaluation of reactive dyestuffs, auxiliaries and selected effluents in textile finishing industry to luminescent bacteria Vibrio fischeri, Chemosphere, 46 (2002) 339–344.
[6] H.A. Mekkawy, M.O. Ali, A.M. El-Zawahry, OP3A18-Toxic effect of synthetic and natural food dyes on renal and hepatic functions in rats, Toxicol. Lett., 95 (1998) 155–161.
[7] S. Raghu, C.W. Lee, S. Chellammal, S. Palanichamy, C.A. Basha, Evaluation of electrochemical oxidation techniques for degradation of dye effluents-A comparative approach, J. Hazard. Mater., 171 (2009) 748–754.
[8] P. Kariyajjanavar, N. Jogttappa, Y.A. Nayaka, Studies on degradation of reactive textile dyes solution by electrochemical method, J. Hazard. Mater., 190 (2011) 952–961.
[9] M.M. Haque, W.T. Smith, D.K.Y. Wong, Conducting polypyrrole films as a potential tool for electrochemical treatment of azo dyes in textile wastewaters, J. Hazard. Mater., 283 (2015) 164–170.
[10] E. Hu, X. Wu, S. Shang, X.M. Tao, S.X. Jiang, L. Gan, Catalytic ozonation of simulated textile dyeing wastewater using mesoporous carbon aerogel supported copper oxide catalyst, J. Clean Prod., 112 (2016) 4710–4718.
[11] P. Aravinda, H. Selvaraj, S. Ferro, M. Sundaram, An integrated (electro- and bio-oxidation) approach for remediation of industrial wastewater containing azo-dyes: Understanding the degradation mechanism and toxicity assessment, J. Hazard. Mater., 318 (2016) 203–215.
[12] C. Zhang, L. Ai, J. Jiang, Solvothermal synthesis of MIL-53(Fe) hybrid magnetic composites for photoelectrochemical water oxidation and organic pollutant photodegradation under visible light, J. Mater. Chem. A, 3 (2015) 3074–3081.
[13] M.S. MohyEldin, K.M. Aly, Z.A. Khan, A.E. Meky, T.S. Saleh, A.S. Elbogamy, Development of novel acid-base ions exchanger for basic dye removal: phosphoric acid doped pyrazole-g-polyglycidyl methacrylate, Desal. Water Treat. 57/50 (2016) 24047–24055.
[14] X. Cheng, N. Li, M. Zhou, L. Zhang, Y. Deng, Positively charged microporous ceramic membrane for the removal of titan yellow through electrostatic adsorption, J. Environ. Sci., 44 (2016) 204–212.
[15] N. Ghaemi, S.S. Madaeni, P. Daraei, H. Rajabi, T. Shojaeimehr, F. Rahimpour, B. Shirvani, PES mixed matrix nanofiltration membrane embedded with polymer wrapped MWCNT: Fabrication and performance optimization in dye removal by RSM, J. Hazard. Mater., 298 (2015) 111–121.
[16] L. Lu, J. Li, D.H.L. Ng, P. Yang, P. Song, M. Zuo, Synthesis of novel hierarchically porous Fe_3O_4@MgAl-LDH magnetic microspheres and its superb adsorption properties of dye from water, J. Ind. Eng. Chem., 46 (2017) 315–323.
[17] S. Chong, G. Zhang, H. Tian, H. Zhao, Rapid degradation of dyes in water by magnetic Fe^0/Fe_3O_4/graphene composites, J. Environ. Sci., 44 (2016) 148–157.
[18] M. Akgül, A. Karabakan, Promoted dye adsorption performance over desilicated natural zeolite, Micropor. Mesopor. Mater., 145 (2011) 157–164.
[19] N. Rajic, D. Stojakovic, S. Jevtic, N.Z. Logar, J. Kovac, V. Kaucic, Removal of aqueous manganese using the natural zeolitic tuff from the VranjskaBanja deposit in Serbia, J. Hazard. Mater., 172 (2009) 1450–1457.
[20] T. Matias, J. Marques, M.J. Quina, L. Gando-Ferreira, A.J.M. Valente, A. Portugal, L. Durães, Silica-based aerogels as adsorbents for phenol-derivative compounds, Colloids Surf. A, 480 (2015) 260–269.
[21] M.A. Tahir, H.N. Bhatti, M. Iqbal, Solar Red and Brittle Blue direct dyes adsorption onto Eucalyptus angophoroides bark: Equilibrium, kinetics and thermodynamic studies, J. Environ. Chem. Eng., 4 (2016) 2431–2439.
[22] A. El-Tayeb, A.H. El-Shazly, M.F. Elkady, A. Abdel-Rahman, Non-thermal plasma as a new advanced technique for intensifying the industrial wastewater treatment, Desal. Water Treat., 61 (2017) 230–239.
[23] M. Shirzad-Siboni, A. Khataee, S.W. Joo, Kinetics and equilibrium studies of removal of an azo dye from aqueous solution by adsorption onto scallop, J. Ind. Eng. Chem., 20 (2014) 610–615.
[24] M. Shirzad-Siboni, S.J. Jafari, O. Giahi, I. Kim, S.M. Lee, J.K. Yang, Removal of acid blue 113 and reactive black 5 dye from aqueous solutions by activated red mud, J. Ind. Eng. Chem., 20 (2014) 1432–1437.

[25] M. Shirzad-Siboni, A. Khataee, A. Hassani, S. Karaca, Preparation, characterization and application of a CTAB-modified nanoclay for the adsorption of an herbicide from aqueous solutions: Kinetic and equilibrium studies, Compt. Rend. Chim., 18 (2015) 204–214.
[26] K. Rasoola, D.S. Lee, Effect of ZnO nanoparticles on biodegradation and biotransformation of co-substrate and sulphonatedazo dye in anaerobic biological sulfate reduction processes, Int. Biodet. Biodeg., 109 (2016) 150–156.
[27] N.M. Mahmoodi, M. Ghezelbash, C. Ghotbei, M. Kazemeini, Bi-amino surface functionalized nanoparticles: synthesis and binary system dye removal from wastewater containing anionic dyes, Desal. Water Treat., 70 (2017) 347–354.
[28] S. Tunç, O. Duman, T. Gürkan, Monitoring the decolorization of acid orange 8 and acid red 44 from aqueous solution using Fenton's reagents by online spectrophotometric method: effect of operation parameters and kinetic study, Ind. Eng. Chem. Res., 52 (2013) 1414–1425.
[29] A. Asfaram, M. Ghaedi, S. Hajati, A. Goudarzi, A.A. Bazrafshan, Simultaneous ultrasound-assisted ternary adsorption of dyes onto copper-doped zinc sulfide nanoparticles loaded on activated carbon: optimization by response surface methodology, Spectrochim. Acta A, 145 (2015) 203–212.
[30] D. Shao, G. Hou, J. Li, T. Wen, X. Ren, X. Wang, PANI/GO as a super adsorbent for the selective adsorption of uranium(VI), Chem. Eng. J., 255 (2014) 604–612.
[31] R. Ansari Khalkhali, R. Omidvari, Adsorption of mercuric ion from aqueous solutions using activated carbon, Pol. J. Environ. Stud., 14 (2005) 185–188.
[32] E. Ayranci, O. Duman, In-Situ UV-Visible spectroscopic study on the adsorption of some dyes onto activated carbon cloth, Sep. Sci. Technol., 44 (2009) 3735–3752.
[33] E. Ayranci, O. Duman, Structural effects on the interactions of benzene and naphthalene sulfonates with activated carbon cloth during adsorption from aqueous solutions, Chem. Eng. J., 156 (2010) 70–76.
[34] O. Duman, S. Tunç, T. G. Polat, Adsorptive removal of triarylmethane dye (Basic Red 9) from aqueous solution by sepiolite as effective and low-cost adsorbent, Microporous Mesoporous Mater., 210 (2015) 176–184.
[35] O. Duman, S. Tunç, T.G. Polat, Determination of adsorptive properties of expanded vermiculite for the removal of C. I. Basic Red 9 from aqueous solution: Kinetic, isotherm and thermodynamic studies, Appl. Clay Sci., 109–110 (2015) 22–32.
[36] O. Duman, S. Tunç, T.G. Polat, B.K. Bozoğlan, Synthesis of magnetic oxidized multiwalled carbon nanotube-κ-carrageenan-Fe_3O_4 nanocomposite adsorbent and its application in cationic Methylene Blue dye adsorption, Carbohydr. Polym., 147 (2016) 79–88.
[37] O. Duman, S. Tunç, B.K. Bozoğlan, T.G. Polat, Removal of triphenylmethane and reactive azo dyes from aqueous solution by magnetic carbon nanotube-κ-carrageenan-Fe_3O_4 nanocomposite, J. Alloys. Comp., 687 (2016) 370–383.
[38] A. Hatamie, H. Parham, B. Zargar, Z. Heidari, Evaluating magnetic nano-ferrofluid as a novel coagulant for surface water treatment, J. Mol. Liq., 219 (2016) 694–702.
[39] X.S. Li, Y.H. Fan, S.W. Zhang, S.H. Qi, Enhanced adsorption removal of anionic dyes via a facile preparation of amino-functionalized magnetic silica, Water Sci. Technol., 75 (2017) 1399–1409.
[40] L. Sun, S. Hu, H. Sun, H. Guo, H. Zhu, M. Liu, H. Sun, Malachite green adsorption onto Fe_3O_4@SiO_2-NH_2: isotherms, kinetic and process optimization, RSC Adv., 5 (2015) 11837–11844.
[41] Z. Xu, W. Li, Z. Xiong, J. Fang, Y. Li, Q. Wang, Q. Zeng, Removal of anionic dyes from aqueous solution by adsorption onto amino-functionalized magnetic nanoadsorbent, Desal. Water Treat., 57 (2016) 7054–7065.
[42] F. Tian, X. Zhang, Y. Chen, Amino-functionalized metal-organic framework for adsorption and separation of dichloromethane and trichloromethane, RSC Adv., 6 (2016) 63895–63904.
[43] Z. Hasan, M. Tong, B.K. Jung, I. Ahmed, C .Zhong, S.H. Jhung, Adsorption of pyridine over amino-functionalized metal-organic frameworks: attraction via hydrogen bonding versus base-base repulsion, J. Phys. Chem. C, 118 (2014) 21049–21056.
[44] K. Nakanishi, M. Tomita, K. Kato, Synthesis of amino-functionalized mesoporous silica sheets and their application for metal ion capture, J. Asian Ceram. Soc., 3 (2015) 70–76.
[45] S. Hao, J. Zhang, Y. Zhong, W. Zhu, Selective adsorption of CO_2 on amino-functionalized silica spheres with centrosymmetric radial mesopores and high amino loading, Adsorption, 18 (2012) 423–430.
[46] X. Li, C. Han, W. Zhu, W. Ma, Y. Luo, Y. Zhou, J. Yu, K. Wei, Cr(VI) Removal from aqueous by adsorption on amine-functionalized mesoporous silica prepared from silica fume, J. Chem., 2014 (2014) 1–10.
[47] N. Fellenz, F.J. Perez-Alonso, P.P. Martin, J.L. García-Fierro, J.F. Bengoa, S.G. Marchetti, S. Rojas, Chromium (VI) removal from water by means of adsorption-reduction at the surface of amino-functionalized MCM-41 sorbents, Micropor. Mesopor. Mat., 239 (2017) 138–146.
[48] S. Hao, A. Verlotta, P. Aprea, F. Pepe, D. Caputo, W. Zhu, Optimal synthesis of amino-functionalized mesoporoussilicas for the adsorption of heavy metal ions, Micropor. Mesopor. Mat., 236 (2016) 250–259.
[49] J. Ou, M. Mei, X. Xu, Magnetic adsorbent constructed from the loading of amino functionalized Fe_3O_4 on coordination complex modified polyoxometalates nanoparticle and its tetracycline adsorption removal property study, J. Solid State Chem., 238 (2016) 182–188.
[50] Y. Wang, R. Qu, F. Pan, X. Jia, C. Sun, C. Ji, Y. Zhang, K. An, Y. Mu, Preparation and characterization of thiol- and amino-functionalized polysilsesquioxane coated poly(p-phenyleneterephthal amide) fibers and their adsorption properties towards Hg(II), Chem. Eng. J., 317 (2017) 187–203.
[51] H.Y. Shen, Z.X. Chen, Z.H. Li, M.Q. Hu, X.Y. Dong, Q.H. Xia, Controlled synthesis of 2,4,6-trichlorophenol-imprinted amino-functionalized nano-Fe_3O_4-polymer magnetic composite for highly selective adsorption, Colloids Surf. A, 481 (2015) 439–450.
[52] N. Yin, K. Wang, L. Wang, Z. Li, Amino-functionalized MOFs combining ceramic membrane ultrafiltration for Pb(II) removal, Chem. Eng. J., 306 (2016) 619–628.
[53] M. Hadavifar, N. Bahramifar, H. Younesi, Q. Li, Adsorption of mercury ions from synthetic and real wastewater aqueous solution by functionalized multi-walled carbon nanotube with both amino and thiolated groups, Chem. Eng. J., 237 (2014) 217–228.
[54] N.M. Mahmoodi, F. Bagherpour, E. Nariyan, Amine functionalization; Magnetic carbon nanotube; Synthesis; Binary system dye removal, Desal. Water Treat., 56 (2015) 107–120.
[55] S. Tunç, T. Gürkan, O. Duman, On-line spectrophotometric method for the determination of optimum operation parameters on the decolorization of Acid Red 66 and Direct Blue 71 from aqueous solution by Fenton process, Chem. Eng. J., 181–182 (2012) 431–442.
[56] J.P. Koplan, Toxicological profile for benzidine. U.S. Department of health and human services public health service agency for toxic substances and disease registry, September 2001.
[57] N.O. Mahmoodi, A. Ghavidast, S. Mirkhaef, M.A. Zanjanchi, Photochromism of azobenzene-thiol-1,3-diazabicyclo-[3.1.0] hex-3-ene on silver nanoparticles, Dyes Pigments, 118 (2015) 110–117.
[58] M. Mohammadi Galangash, Z. Niyazi Kolkasaraei, A. Ghavidast, M. Shirzad-Siboni, Facile synthesis of methyl propylaminopropanoate functionalized magnetic nanoparticles for removal of acid red 114 from aqueous solution, RSC Adv., 6 (2016) 113492–113502.
[59] N.O. Mahmoodi, A. Ghavidast, N. Amirmahani, A comparative study on the nanoparticles for improved drug delivery systems, J. Photochem. Photobiol. B. Biol., 162 (2016) 681–693.

[60] A. Ghavidast, N.O. Mahmoodi, M.A. Zanjanchi, Synthesis and photochromic properties of disulfide-1,3-diazabicyclo [3.1.0] hex-3-ene functionalized silver nanoparticles, J. Mol. Liq., 198 (2014) 128–133.
[61] B.D. Cullity, Elements of X-ray Diffraction, Addison-Wesley, Reading, MA, 1967.
[62] L. Zhang, H. Zhang, W. Guo, Y. Tian, Removal of malachite green and crystal violet cationic dyes from aqueous solution using activated sintering process red mud, Appl. Clay. Sci., 93 (2014) 85–93.
[63] H. Li, D. Xiao, H. He, R. Lin, P. Zuo, Adsorption behavior and adsorption mechanism of Cu(II) ions on amino-functionalized magnetic nanoparticles, Trans. Nonferrous Met. Soc. China, 23 (2013) 2657–2665.
[64] F. Liu, X.G. Luo, X.Y. Lin, Adsorption of tannin from aqueous solution by deacetylated konjac glucomannan, J. Hazard. Mater., 178 (2010) 844–850.
[65] J.F. Gao, Q. Zhang, K. Su, R.N. Chen, Y.Z. Peng, Biosorption of Acid Yellow 17 from aqueous solution by non-living aerobic granular sludge, J. Hazard. Mater., 174 (2010) 215–225.
[66] Y. Önal, C. Akmil-Başar, Ç. Sarıcı-Özdemir, Investigation kinetics mechanisms of adsorption malachite green onto activated carbon, J. Hazard. Mater., 146 (2007) 194–203.
[67] M. Bhaumik, T.Y. Leswifi, A. Maity, V.V. Srinivasu, M.S. Onyango, Removal of fluoride from aqueous solution by polypyrrole/Fe_3O_4 magnetic nanocomposite, J. Hazard. Mater., 186 (2011) 150–159.
[68] I. Langmuir, The adsorption of gases on plane surfaces of glass, mica and platinum, J. Am. Chem., 0 (1918) 1361–1403.
[69] E. Bulut, M. Özacar, İ.A. Şengil, Equilibrium and kinetic data and process design for adsorption of congo red onto bentonite, J. Hazard. Mater., 154 (2008) 613–622.
[70] S. Senthilkumaar, P. Kalaamani, K. Porkodi, P.R. Varadarajan, C.V. Subburaam, Adsorption of dissolved Reactive red dye from aqueous phase onto activated carbon prepared from agricultural waste, Bioresour. Technol., 97 (2006) 1618–1625.
[71] O. Duman, E. Ayranci, Attachment of benzo-crown ethers onto activated carbon cloth to enhance the removal of chromium, cobalt and nickel ions from aqueous solutions by adsorption, J. Hazard. Mater., 176 (2010) 231–238.
[72] O. Duman, E. Ayranci, Adsorptive removal of cationic surfactants from aqueous solutions onto high-area activated carbon cloth monitored by in situ UV spectroscopy, J. Hazard. Mater., 174 (2010) 359–367.
[73] I. Langmuir, The constitution and fundamental properties of solids and liquids. part I. solids, J. Am. Chem. Soc., 38 (1916) 2221–2295.
[74] N. Kannan, M.M. Sundaram, Kinetics and mechanism of removal of methylene blue by adsorption on various carbons-a comparative study, Dyes Pigments, 51 (2001) 25–40.
[75] M.A.K.M. Hanafiah, W.S.W. Ngah, S.H. Zolkafly, L.C. Teong, Z.A.A. Majid, Acid blue 25 adsorption on base treated shoreadasyphylla sawdust: kinetic, isotherm, thermodynamic and spectroscopic analysis, J. Environ. Sci., 24 (2012) 261–268.
[76] H. Freundlich, Über die Adsorption in Lösungen, W. Engelmann, 1906.
[77] L. Fan, Y. Zhang, X. Li, C. Luo, F. Lu, H. Qiu, Removal of alizarin red from water environment using magnetic chitosan with alizarin red as imprinted molecules, Colloids Surf. B: Biointerfaces, 91 (2012) 250–257.
[78] L. Ai, C. Zhang, Z. Chen, Removal of methylene blue from aqueous solution by a solvothermal-synthesized graphene/magnetite composite, J. Hazard. Mater., 192 (2011) 1515–1524.
[79] L. Xiong, Y. Yang, J. Mai, W. Sun, C. Zhang, D. Wei, Q. Chen, Adsorption behavior of methylene blue onto titanate nanotubes, J. Ni, Chem. Eng. J., 156 (2010) 313–320.
[80] G. Mc Kay, A. Mesdaghinia, S. Nasseri, M. Hadi, M. SolaimanyAminabad, Optimum isotherms of dyes sorption by activated carbon: fractional theoretical capacity & error analysis, Chem. Eng. J., 251 (2014) 236–247.
[81] N. Rajamohan, M. Rajasimman, R. Rajeshkannan, B. Sivaprakash, Kinetic modeling and isotherm studies on a batch removal of acid red 114 by an activated plant biomass, J. Eng. Sci. Technol., 8 (2013) 778–792.
[82] G. Revathi, S. Ramalingam, P. Subramanian, A. Ganapathi, R. Valliappan, Adsorptive removal of Acid Red-114 dye by activated carbon prepared from Kattamanakku tree leaves, Oriental. J. Chem., 26 (2010) 1385–1391.
[83] K. Geetha, N. Velmani, P.S. Syed Shabudeen, Estimation of acid red 114 adsorption using Ceiba Pentandra wood bark based activated carbon modified using phosphoric acid, J. Chem. Pharm. Res., 6 (2014) 26–39.
[84] K. Geetha, N. Velmani, A. Manimaran, K. Mabel Hebsuba, S. Karthikeyan, Non-commercial agro waste product for the removal of acid red-114 using ipomeacarnea stem waste, J. Environ. Nanotechnol., 5 (2016) 39–45.
[85] N. Thinakaran, P. Panneerselvam, P. Baskaralingam, D. Elango, S. Sivanesan, Equilibrium and kinetic studies on the removal of acid red 114 from aqueous solutions using activated carbons prepared from seed shells, J. Hazard. Mater., 158 (2008) 142–150.
[86] M. Anbia, S. Salehi, Removal of acid dyes from aqueous media by adsorption onto amino-functionalized nanoporous silica SBA-3, Dyes Pigments, 94 (2012) 1–9.
[87] G. Kaykioglu, E. Gunes, Comparison of acid red 114 dye adsorption by Fe_3O_4 and Fe_3O_4 impregnated rice husk ash, J. Nanomater., (2016) DOI: 10.1155/2016/6304096.